Journal of Alloys and Compounds, 203 (1994) 209–216
JALCOM 890

Synthesis, high resolution electron microscopy and crystal structure refinement of the cluster compound $Ba_3Nb_{16}O_{23}$ by X-ray and neutron diffraction

V.G. Zubkov, V.A. Pereleyaev, A.P. Tyutyunnik, I.A. Kontsevaya and V.I. Voronin
Institute of Solid State Chemistry, Russian Academy of Sciences, Pervomayskaya 91, 620219 Ekaterinenburg, GSP-145 (Russian Federation)

G. Svensson*
Arrhenius Laboratory, Department of Inorganic Chemistry, Stockholm University, S-106 91 Stockholm (Sweden)

(Received June 21, 1993)

Abstract

$Ba_3Nb_{16}O_{23}$ was prepared by reducing a mixture of $BaCO_3$ and Nb_2O_5 with acetylene soot under vacuum at 1550–1600 °C. The structure was determined from high resolution electron microscopy images and was refined by the Rietveld technique using X-ray and neutron powder diffraction data. The unit cell parameters are $a = 20.9301(4)$ Å, $b = 12.4785(3)$ Å and $c = 4.1619(1)$ Å, space group *Cmmm*, $Z = 2$. The crystal structure can be described as an intergrowth of $BaNbO_3$ and NbO. Characteristic building units are quadruple chains of corner-sharing Nb_6 octahedra connected via columns with a perovskite-type structure to form a three-dimensional network.

1. Introduction

Investigations of the phase relations among the reduced oxoniobates have revealed the existence of a large number of compounds containing Nb_6O_{12} clusters. These compounds have recently been discussed in a review article [1]. The Nb_6O_{12} cluster unit consists of a central Nb_6 octahedron with 12 oxygen atoms capping the edges. Typical Nb–Nb and Nb–O bond lengths are 2.8–3.0 and 2.0–2.2 Å respectively. The Nb_6O_{12} clusters can condense via corner sharing of the central Nb_6 octahedra in one, two or three dimensions. The degree of condensation, the Nb–Nb bond lengths as well as the valence of the Nb atoms are effects of the electron distribution in the compound.

A number of compounds with one- or two-dimensionally infinite condensation of Nb_6O_{12} clusters have been found in the BaO–NbO–NbO_2 system. Their structures can all be described as intergrowths of $BaNbO_3$ (perovskite type [2–4]) and NbO units. NbO has an ordered deficient NaCl-type structure [5] but can alternatively be described as a three-dimensionally infinite condensation of Nb_6O_{12} clusters [6]. For a clearer discussion of these intergrowth phases a notation has been introduced [1] which describes the size of the NbO and perovskite type units by the matrices $[p*q*r]$ and $\{s*t*u\}$ respectively. NbO has the description $[\infty*\infty*\infty]$, $\{0*0*0\}$ and $BaNbO_3$ the description $[0*0*0]$, $\{\infty*\infty*\infty\}$, while $BaNb_8O_{14}$ [7, 8] with discrete Nb_6O_{12} clusters is described by $[1*1*1]$.

Various degrees of condensation have been found. The simplest example of one-dimensional condensation is found in the single chains of Nb_6O_{12} clusters and $BaNbO_3$ units of $BaNb_5O_8$ ($[1*1*\infty]$, $\{1*1*\infty\}$) [9]. The triple NbO and quadruple perovskite chains present in $Ba_4Nb_{14}O_{23}$ ($[1*3*\infty]$, $\{2*2*\infty\}$) [10, 11] and the quadruple chains in $Ba_4Nb_{17}O_{26}$ ($[2*2*\infty]$, $\{2*2*\infty\}$) [12] represent the first steps towards the two-dimensionally infinite condensations in $Ba_2Nb_5O_9$ ($[1*\infty*\infty]$, $\{2*\infty*\infty\}$) [13–15], $BaNb_4O_6$ ($[1*\infty*\infty]$, $\{1*\infty*\infty\}$) [14, 15] and $BaNb_7O_9$ ($[2*\infty*\infty]$, $\{1*\infty*\infty\}$) [16]. Most of these compounds have to be synthesized at rather high temperatures (above 1250 °C), since at lower temperatures a quasi-ordered intergrowth of NbO and $BaNbO_3$ forms, the so-called *α phasoid* [17, 18].

The present paper discusses the synthesis and crystal structure of the new compound $Ba_3Nb_{16}O_{23}$ containing $\{1*3*\infty\}$ perovskite blocks and $[2*2*\infty]$ NbO blocks. Microregions of this structure have earlier been observed by high resolution electron microscopy (HREM) studies of α phasoid crystallites [1, 18].

*Author to whom correspondence should be addressed.

SSDI 0925-8388(93)00890-B

2. Experimental details

$Ba_3Nb_{16}O_{23}$ was synthesized from $BaCO_3$ (99.99%) and Nb_2O_5 (99.999%) with acetylene soot (C 99.99%) as reductant. The mixture was pressed into pellets which were placed in a graphite crucible lined with tantalum foil. The crucible with the sample was annealed in a vacuum (less than 10^{-8} Pa) furnace with tungsten windings. The temperature was increased stepwise from 1200 to 1600 °C.

For the electron microscopy studies small amounts of the sample were crushed in butanol. A drop of the dispersion was put on a holey carbon film supported by a copper grid. Electron diffraction studies and microanalysis of single-crystallite fragments were performed in a Jeol JEM-2000FX microscope operating at 200 kV (±45° side-entry double-tilt holder). The microscope was equipped with a Link QX200 energy-dispersive detector (EDS) in the high angle (70°) position. The HREM studies were performed in a Jeol JEM-200CX with a top-entry double-tilt goniometer (±10°, 2.4 Å point-to-point resolution) operated at 200 kV. The program suite SHRLI [19] was used for theoretical HREM simulations.

X-ray powder diffraction data were collected with a Stoe STADI-P diffractometer with a rotating sample in symmetrical transmission mode. A germanium crystal monochromator (Cu $K\alpha_1$ radiation) and a position-sensitive scintillation detector (collecting angle $2\theta \approx 43.5°$, angular increment 0.015°, counting time 30 min) were used. The 2θ range was 5°–110° and the stepwise scanning interval 5°. The intensity non-linearity of the central part (about 12°) of the detector was better than about 1%. Separate diffraction patterns ($\Delta(2\theta) = 5°$) obtained by this technique were combined to create a complete diffraction pattern.

Neutron diffraction data were collected at room temperature on a set-up with a 10-detector registration system [20]. The wavelength ($\lambda = 1.528$ Å, obtained with a double monochromator based on pyrolytic graphite (002) and a germanium (111) crystal) was calibrated with electrolytic copper powder. For data collection a 30 g powder sample of $Ba_3Nb_{16}O_{23}$ was placed in a container (radius 4 mm, length 40 mm) made of aluminium foil (0.02 mm). The pattern was collected in 0.1° steps from 5° to 110°.

The program DBW 4.1. was used [21] for the Rietveld refinements based on both the X-ray and neutron diffraction data sets.

3. Results

The phase analysis (X-ray powder and electron diffraction) showed that the α phasoid [18] and NbO form in the temperature range 1200–1450 °C. It is often difficult to determine the presence of the α phasoid from X-ray powder diffraction patterns owing to overlap with lines of ordered phases present. However, the α phasoid has a very characteristic electron diffraction pattern along ⟨001⟩, exhibiting a tetragonal subcell $a \approx c \approx 4.2$ Å (see Fig. 1). The subcell reflections exhibit the systematic absences $h+k \neq 2n$, indicating C centring. Around all subreflection positions, present as well as absent, satellite spots are seen. They occur in two different directions, for even and odd $(h+k)_{sub}$. In the X-ray powder pattern the reflections corresponding to NbO decrease in intensity when the synthesis temperature is increased, which indicates that NbO dissolves in the α phasoid at higher temperatures. The formation of $Ba_3Nb_{16}O_{23}$ starts at 1450 °C and ends at 1550–1600 °C according to the X-ray diffraction patterns. Numerous experiments have shown that $Ba_3Nb_{16}O_{23}$ is only obtained after complete dissolution of NbO in the α phasoid. This supports the central role of the α phasoid during the formation of intergrowth phases between $BaNbO_3$ and NbO. A similar reaction path has been found for $Ba_4Nb_{17}O_{26}$ [12].

The HREM studies show that the formation of $Ba_3Nb_{16}O_{23}$ starts as small domains in the α phasoid crystallites. An HREM image of an α phasoid crystallite is shown in Fig. 2 together with an interpretation. It was found in a sample with the composition $Ba_{0.8}Nb_4O_6$ heated to 1200 °C. The interpretation of the HREM image is rather straightforward [18]. The crosses correspond to Nb octahedra in the NbO blocks and the smaller spots in between to Ba and Nb atoms in the perovskite blocks. In the HREM image and in the interpretation some small domains of $Ba_3Nb_{16}O_{23}$ and $Ba_4Nb_{17}O_{26}$ are marked. These grow as the synthesis

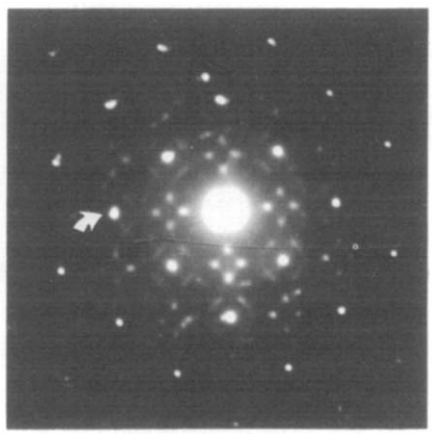

Fig. 1. Typical ED pattern of an α phasoid crystallite found in a sample with nominal composition $Ba_{0.8}Nb_4O_6$ synthesized at 1200 °C. The ED pattern indicates a C-centred subcell with $a \approx 4.2$ Å. One subcell spot $(200)_{sub}$ is arrowed. Around the subcell reflections, diffuse satellite spots are seen in two different directions depending on $(h+k)_{sub}$ being even or odd.

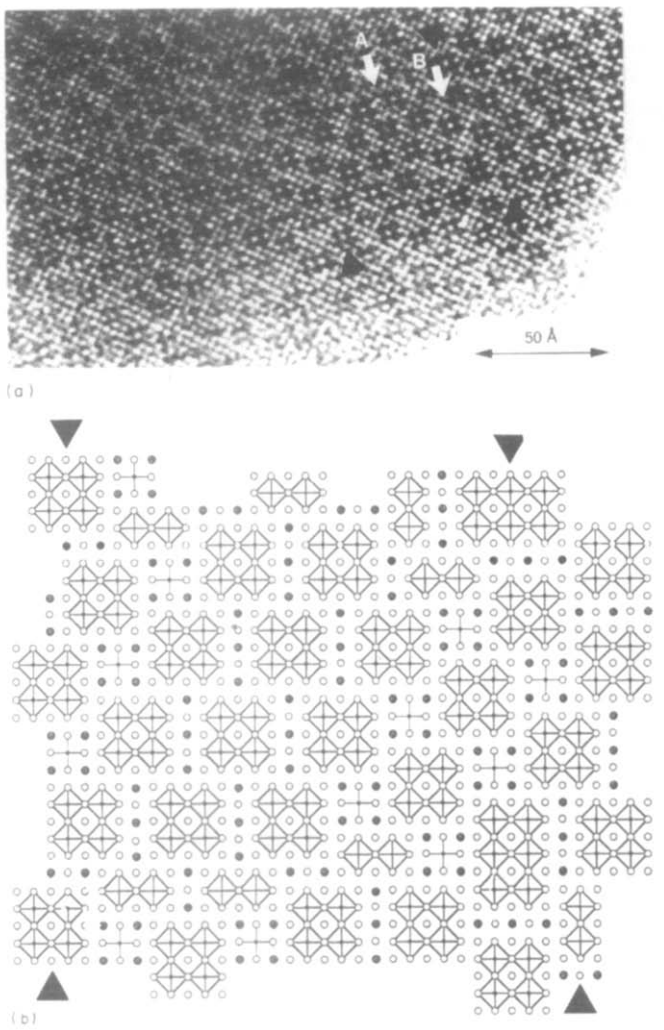

Fig. 2. (a) HREM image of a typical α phasoid crystallite found in the same sample as in Fig. 1. The NbO blocks are seen as large spots or crosses and the Ba and Nb atoms in the perovskite blocks as smaller spots in between. Two small domains of $Ba_3Nb_{16}O_{23}$ and $Ba_4Nb_{17}O_{26}$ are marked A and B respectively in the image. (b) Interpretation of the marked (filled triangles) region in (a).

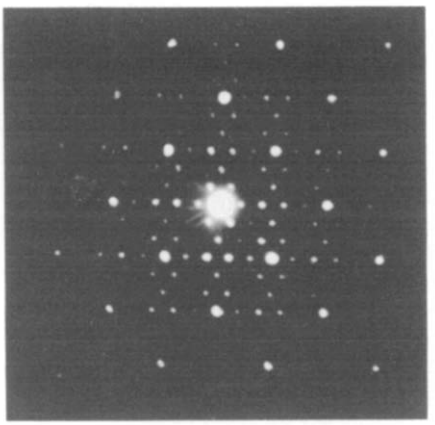

Fig. 3. ED pattern of $Ba_3Nb_{16}O_{23}$ taken along $\langle 001 \rangle$. The systematic absence $h+k \neq 2n$ indicates a C-centred unit cell.

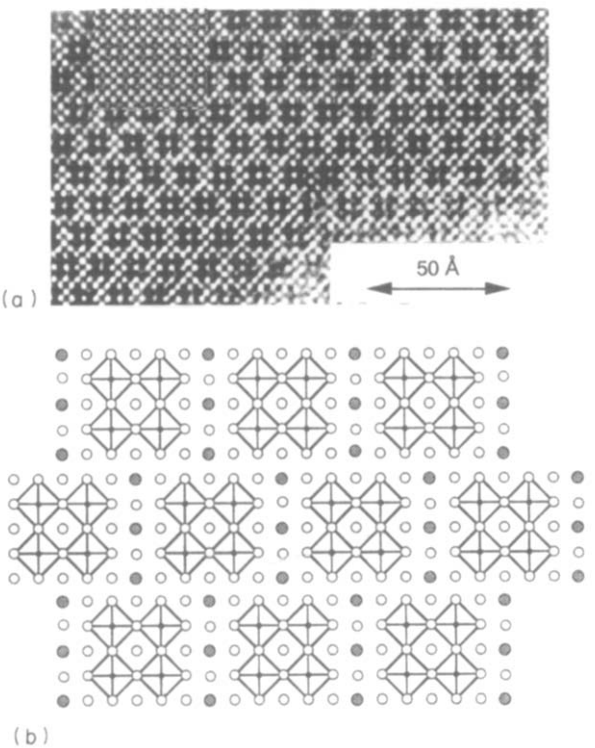

Fig. 4. (a) HREM image of a $Ba_3Nb_{16}O_{23}$ crystallite along $\langle 001 \rangle$ found in a sample with the nominal composition $Ba_3Nb_{16}O_{23}$ synthesized at 1550 °C. (b) A structure model of $Ba_3Nb_{16}O_{23}$ derived from the HREM image. The corresponding simulated HREM image is inserted in (a).

temperature is increased. Similar domains have been observed during the HREM study of the formation of $Ba_4Nb_{14}O_{23}$ [10].

The electron diffraction (ED) studies showed $Ba_3Nb_{16}O_{23}$ to have a C-centred unit cell with $a \approx 20.9$ Å, $b \approx 12.5$ Å and $c \approx 4.2$ Å. An ED pattern of $Ba_3Nb_{16}O_{23}$ along $\langle 001 \rangle$ is shown in Fig. 3. This cell was refined from the X-ray powder diffraction data to $a = 20.9301(4)$ Å, $b = 12.4785(3)$ Å and $c = 4.1619(1)$ Å. The indexed X-ray pattern is given in Table 1.

An HREM image of $Ba_3Nb_{16}O_{23}$ viewed along $\langle 001 \rangle$ is shown in Fig. 4(a). The interpretation leads to the structural model (space group *Cmmm*) shown in Fig. 4(b). The corresponding simulated HREM image is inserted in the HREM image. The EDS analysis of individual crystallites in the transmission electron microscope using the thin crystal approximation (neglecting absorption, atomic number and fluorescence effects [22]) gave an Nb/Ba ratio of 5.5 ± 0.5, close to the expected value of 5.3.

Defects, mostly as variations in the block sizes, were frequently found in the HREM images of $Ba_3Nb_{16}O_{23}$. The HREM image and the interpretations in Fig. 5 show $[2*3*\infty]$ and $[1*2*\infty]$ NbO blocks replacing

TABLE 1. Indices of reflections (h, k, l), interplanar distances d and relative intensities for $Ba_3Nb_{16}O_{23}$. Only reflections with $I_{calc}/I_{max} > 1\%$ are given

h k l	d_{calc} (Å)	d_{obs} (Å)	I_{calc}/I_{max}	I_{obs}/I_{max}
1 1 0	10.7182		13	
2 0 0	10.4650		6	
0 2 0	6.2393	6.24	4	4
2 2 0	5.3591	5.36	2	3
4 0 0	5.2325	5.23	11	10
0 0 1	4.1619	4.16	11	10
1 3 0	4.0797	4.08	13	7
4 2 0	4.0092	4.01	8	7
5 1 0	3.9687	3.969	7	7
1 1 1	3.8797	3.879	8	8
3 3 0	3.5727	3.573	2	2
6 0 0	3.4883		1	
0 2 1	3.4623	3.462	17	18
2 2 1	3.2871	3.287	7	6
6 2 0	3.0440	3.045	1	1
5 3 0	2.9505	2.950	100	100
1 3 1	2.9134	2.913	66	65
4 2 1	2.8874	2.887	36	38
5 1 1	2.8722	2.872	92	89
3 3 1	2.7109	2.711	8	7
4 4 0	2.6795	2.679	1	2
0 4 1	2.4962	2.496	8	7
6 2 1	2.4574	2.4574	26	24
2 4 1	2.4281	2.4281	2	3
5 3 1	2.4070	2.4070	46	46
4 4 1	2.2530	2.2530	17	16
5 5 0	2.1436	2.1436	1	2
1 5 1	2.1293	2.1293	1	1
7 3 1	2.0971	2.0971	4	6
10 0 0	2.0930	2.0930	68	67
8 2 1	2.0873	2.0874	4	4
0 0 2	2.0810	2.0810	69	70
0 6 0	2.0798	2.0797	68	69
6 4 1	2.0300	2.0300	14	12
9 3 0	2.0299		1	
9 1 1	2.0038	2.0038	1	1
4 0 2	1.9336		1	
4 6 0	1.9327		1	
5 5 1	1.9057	1.9057	37	36

the $[2*2*\infty]$ NbO blocks in $Ba_3Nb_{16}O_{23}$. In connection with the $[1*2*\infty]$ defects, contrast variations are seen in the image (marked as unfilled triangles in the image and the interpretation). These probably indicate the presence of defects along the line of sight. However, ED studies of α phasoid crystallites have shown that defects along the c axis do not occur frequently [18]. An HREM image showing a rather unusual intergrowth of a BaO plane {110} in $Ba_3Nb_{16}O_{23}$ is shown in Fig. 6 together with an interpretation.

4. Structure refinement

The approximate structural model obtained from the HREM image in Fig. 4(a) was refined by the Rietveld technique using the X-ray data set. The result is given in Table 2, with a list of I_{obs} and I_{calc} in Table 1. Since with X-rays the detection of light atoms (here oxygen) in the presence of heavy atoms is difficult, neutron powder diffraction was employed to obtain better details of the structure. The atomic coordinates from the X-ray refinement were used as starting coordinates for the Rietveld refinement using the neutron diffraction data. The result is presented in Table 2. Severe correlation was observed for both the X-ray and neutron data sets. A comparison of the results from the X-ray and neutron data sets shows that the positional parameters obtained for the Nb(1), Nb(3) and O atoms, as well as the Debye–Waller factors, differ significantly between the refinements. There may be various reasons for this problem: (i) the large number (21) of structural parameters; (ii) the presence of structural defects in the crystallites as shown in the HREM images above; (iii) the presence of small amounts of the α phasoid in the samples distorting the peak intensities. Both data sets result in atomic coordinates giving some dubious bond lengths compared with what is normally observed for reduced oxoniobates. Since the Ba and Nb positions are better determined from the X-ray data set, it was decided to use the X-ray data for those atoms and the neutron data for the O atoms. This mixed atomic coordinate list gives more reasonable bond lengths (see Table 3) and will be used below.

5. Structure description and discussion

A projection of the $Ba_3Nb_{16}O_{23}$ structure on the xy plane is shown in Fig. 7. It can be described as an intergrowth of quadruple NbO $[2*2*\infty]$ and triple perovskite $BaNbO_3$ $\{1*3*\infty\}$ blocks. The existence of the perovskite blocks is not obvious on a first glance at the structure. An alternative description using Ba_3O_2 slabs may seem more appropriate. However, such a description does not take into account the relation with the structure of $Ba_4Nb_{14}O_{23}$ [11]. This oxide has a structure that is the reverse of $Ba_3Nb_{16}O_{23}$. There are clearly recognizable quadruple perovskite blocks, $\{2*2*\infty\}$, and triple NbO blocks, $[1*3*\infty]$. The unit cell parameters for $Ba_4Nb_{14}O_{23}$ ($a=20.782(4)$ Å, $b=12.448(3)$ Å and $c=4.147(1)$ Å) are very close to those found for $Ba_3Nb_{16}O_{23}$.

In $Ba_3Nb_{16}O_{23}$ the Nb(1), Nb(2), Nb(3), O(1), O(2) and O(3) atoms in the NbO blocks have a coordination as in NbO. The Nb atoms have a planar 4-coordination of O atoms and an 8-coordination of Nb atoms (forming a tetragonal prism). The reverse coordination is found around the O atoms. The Nb(4) and Nb(5) atoms completing the Nb_6 octahedra are (4+1)-coordinated by O atoms, forming square pyramids, and 4-coordinated

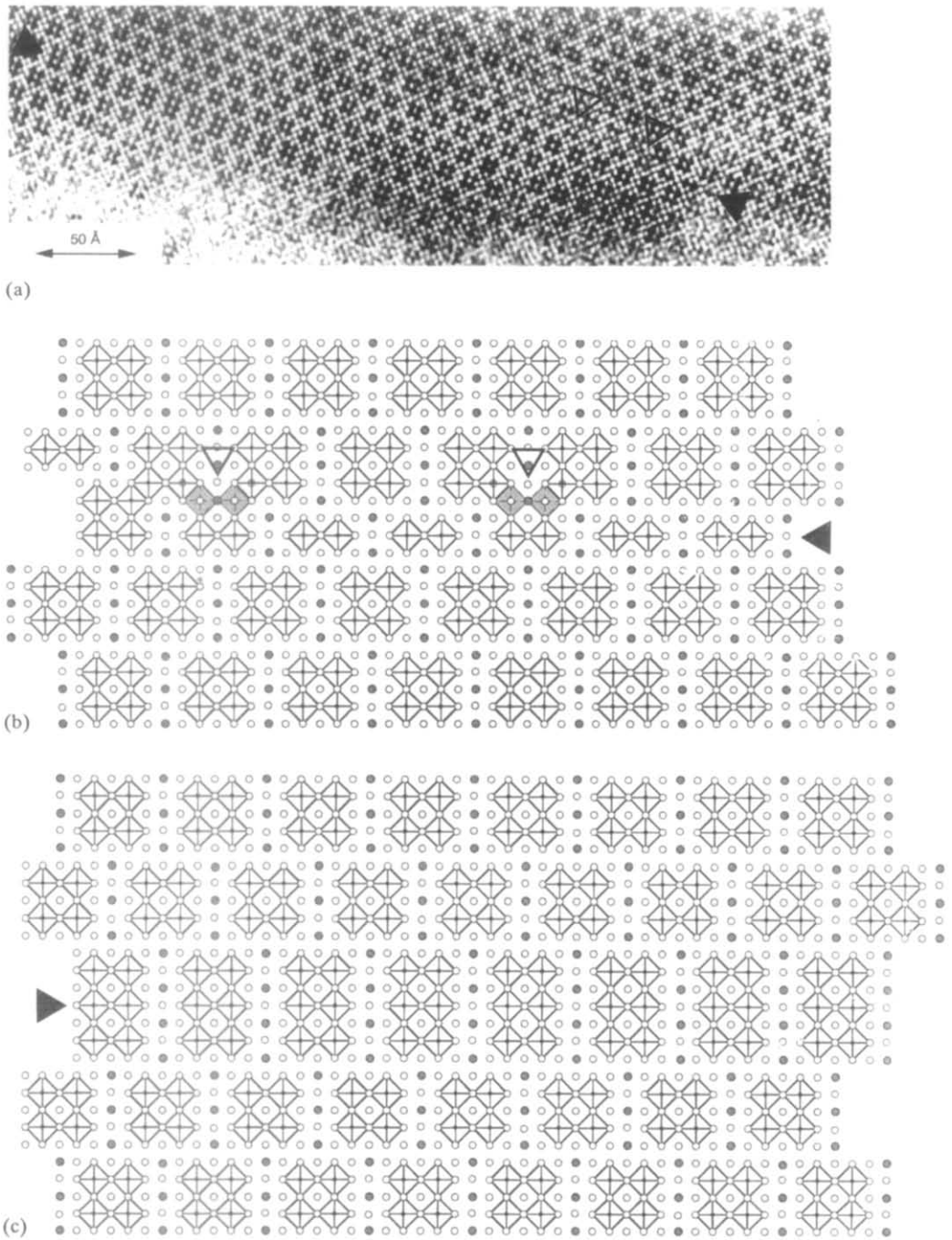

Fig. 5. HREM image of defects found in $Ba_3Nb_{16}O_{23}$ crystallites and corresponding interpretations. (a) Intergrowth of [2∗3∗∞] and [1∗2∗∞] (marked with filled triangles) in the [2∗2∗∞] NbO blocks in $Ba_3Nb_{16}O_{23}$. In connection with the [1∗2∗∞] NbO blocks contrast variations are seen (marked with unfilled triangles). These contrast variations suggest that the blocks do not extend throughout the crystallite in the viewing direction. (b) Interpretation of the HREM image area showing [1∗2∗∞] intergrowth (marked with a filled triangle) and the diffuse contrast (marked with an open triangle) indicating defects along the line of sight. (c) Interpretation of the HREM image area showing [2∗3∗∞] intergrowth (marked with a filled triangle) in $Ba_3Nb_{16}O_{23}$.

by niobium as in a discrete Nb_6O_{12} cluster. The Ba atoms are surrounded by 12 O atoms forming a cubo-octahedron as in perovskite-type $BaNbO_3$.

In $Ba_3Nb_{16}O_{23}$, the Nb–Nb bond lengths range between 2.844 and 2.978 Å (Nb–Nb average 2.928 Å), which is close to the values found in $Ba_4Nb_{17}O_{26}$ (2.795–2.979 Å, average 2.914 Å [12]) and $Ba_4Nb_{14}O_{23}$ (2.841–3.001 Å, average 2.905 Å [11]). In all compounds found so far containing condensed Nb_6O_{12} clusters, the Nb–Nb interatomic distances between Nb atoms linking

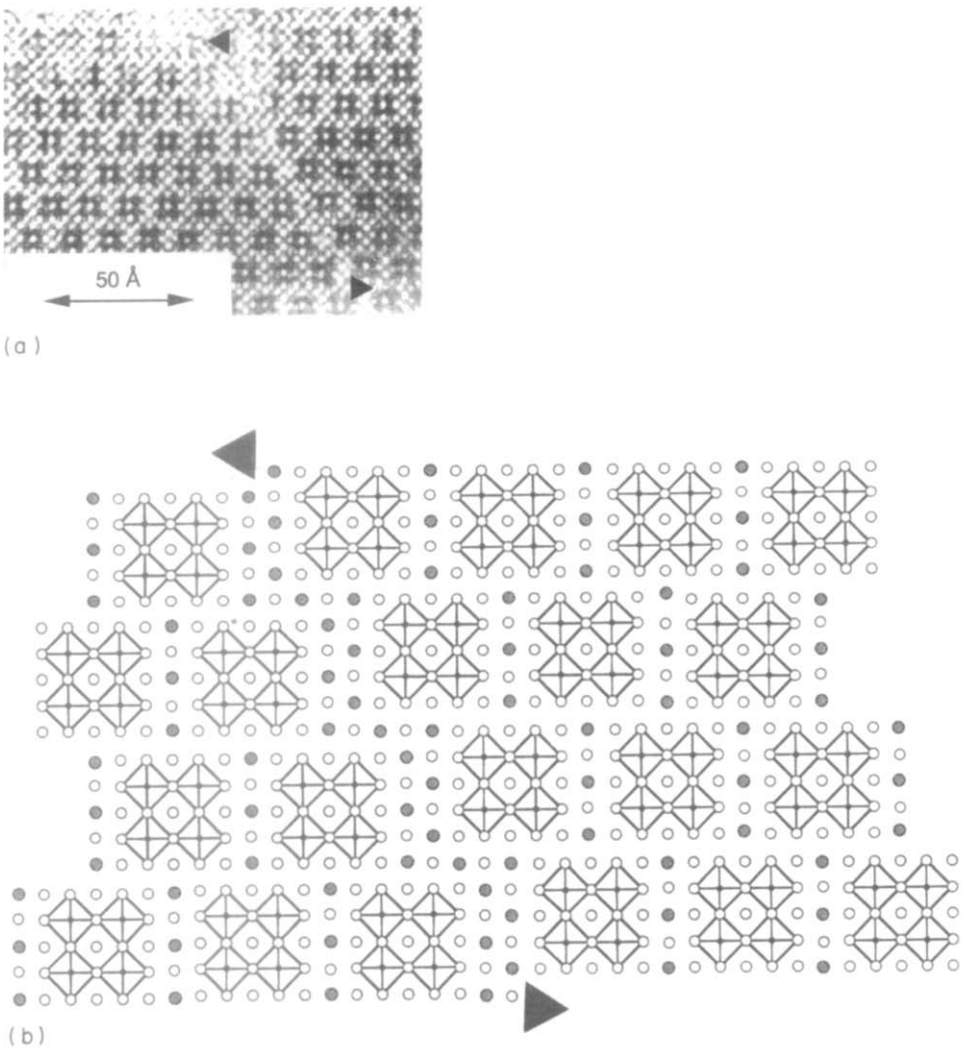

Fig. 6. (a) HREM image showing intergrowth of a BaO layer along {110} in $Ba_3Nb_{16}O_{23}$. (b) The corresponding interpretation. The defect is marked in both the HREM image and the interpretation.

TABLE 2. Crystallographic data, atomic parameters and isotropic temperature factors[a] for $Ba_3Nb_{16}O_{23}$

Space group	*Cmmm*		
a, *b*, *c* (Å)	20.9301(4),	12.4785(3),	4.1619(1)
Cell volume (Å^3)	1086.99		
Unit cell mass (a.m.u.)	4532.7		
Calculated density (g cm^{-3})	6.924		
	X-Ray data	Neutron data	
Number of lines	361	366	
Profile function	Pseudo-Voigt	Gaussian	
FWHM parameters			
U	0.1032(77)	0.5688(474)	
V	−0.0916(87)	−0.8200(776)	
W	0.0778(22)	0.5717(296)	
Asymmetry parameter	0.7784(542)	0.1525(0.1289)	
R_{pf}, R_{wp}	5.11, 5.20	6.17, 9.95	
R_I	8.13	8.08	

(*continued*)

TABLE 2. (*continued*)

Atom	Position	X-Ray data			Neutron data		
		x/a	*y/b*	*z/c*	*x/a*	*y/b*	*z/c*
Ba(1)	2*a*	0	0	0	0	0	0
Ba(2)	4*g*	0.2009(2)	0	0	0.2012(11)	0	0
Nb(1)	4*j*	0	0.3321(6)	½	0	0.3319(10)	½
Nb(2)	8*p*	0.1018(3)	0.3293(2)	0	0.1029(7)	0.3292(15)	0
Nb(3)	4*h*	0.1006(4)	½	½	0.0931(8)	½	½
Nb(4)	8*q*	0.1002(3)	0.1691(3)	½	0.1002(9)	0.1740(21)	½
Nb(5)	8*q*	0.1953(2)	0.3319(4)	½	0.1965(8)	0.3339(12)	½
O(1)	2*c*	0	½	½	0	½	½
O(2)	4*i*	0	0.3374(38)	0	0	0.3250(12)	0
O(3)	4*g*	0.0976(26)	½	0	0.0896(11)	½	0
O(4)	4*i*	0	0.1795(27)	½	0	0.1584(24)	½
O(5)	8*p*	0.1019(18)	0.1685(20)	0	0.0980(9)	0.1618(13)	0
O(6)	8*q*	0.2003(11)	0.1599(18)	½	0.1953(7)	0.1612(17)	½
O(7)	8*p*	0.3021(13)	0.1608(26)	0	0.3001(9)	0.1601(9)	0
O(8)	4*h*	0.2108(13)	½	½	0.2099(10)	½	½
O(9)	4*h*	0.1219(11)	0	½	0.1034(13)	0	½

[a]Debye–Waller factors Bi_{iso}: X-ray data, −0.2148(306) Å^2, neutron data, 0.165(41) Å^2.

TABLE 3. Selected interatomic distances (Å) in $Ba_3Nb_{16}O_{23}$ using X-ray data for Nb atoms and neutron data for O atoms

Ba(1)–4 O(4)	2.87(2)	Nb(3)–2 Nb(1)	2.970(8)
4 O(5)	2.93(2)	4 Nb(2)	2.978(2)
4 O(9)	3.00(2)	2 Nb(5)	2.886(7)
		O(1)	2.106(8)
Ba(2)–2 O(5)	3.01(2)	2 O(3)	2.094(3)
4 O(6)	2.90(2)	O(8)	2.29(2)
2 O(7)	2.88(2)		
2 O(8)	2.80(1)	Nb(4)–Nb(1)	2.922(7)
2 O(9)	2.92(2)	2 Nb(2)	2.886(3)
		Nb(5)	2.844(7)
Nb(1)–4 Nb(2)	2.978(4)	O(4)	2.101(7)
2 Nb(3)	2.970(8)	2 O(5)	2.081(1)
2 Nb(4)	2.922(7)	O(6)	1.99(2)
O(1)	2.095(7)	O(9)	2.111(4)
2 O(2)	2.083(1)		
O(4)	2.17(3)	Nb(5)–2 Nb(2)	2.857(5)
		Nb(3)	2.886(7)
Nb(2)–2 Nb(1)	2.978(4)	Nb(4)	2.844(7)
2 Nb(3)	2.978(2)	Nb(5)	3.069(9)
2 Nb(4)	2.886(3)	O(6)	2.29(2)
2 Nb(5)	2.857(5)	O(6)	2.13(2)
O(2)	2.131(6)	2 O(7)	2.086(1)
O(3)	2.145(4)	O(8)	2.120(6)
O(5)	2.01(2)		
O(7)	2.06(2)		

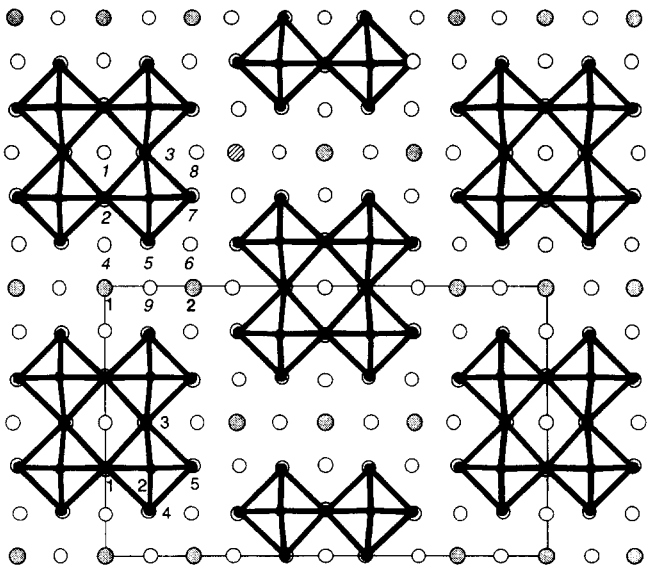

Fig. 7. Crystal structure of $Ba_3Nb_{16}O_{23}$ projected along [001]. Ba atoms (bold numbering) are shown as large hatched, Nb atoms (normal) as filled and O atoms (italic) as unfilled circles.

the Nb_6 octahedra are longer than the remaining Nb–Nb interatomic distances. In $Ba_3Nb_{16}O_{23}$, $BaNb_7O_9$ [16] and $Ba_4Nb_{17}O_{26}$ [12] the central part of the NbO block contains a unit of Nb and O atoms exactly corresponding to the unit cell of NbO (each Nb is surrounded by 8 Nb and 4 O atoms). The volume of this unit in $Ba_3Nb_{16}O_{23}$ (75.6 Å^3), $BaNb_7O_9$ (74.7 Å^3) and $Ba_4Nb_{17}O_{26}$ (74.2 Å^3) is close to that found in NbO (74.6 Å^3).

The uncertainty of the oxygen positions makes a discussion of the Nb–O distances of limited value. However, the Nb–O distances exhibit a somewhat wider distribution (1.99–2.29 Å) than found in other intergrowth compounds between $BaNbO_3$ and NbO. This could reflect the uncertainty in the oxygen positions. The cubo-octahedra of oxygen atoms around the barium atoms are slightly distorted. The average Ba(1)–O and Ba(2)–O distances of 2.93 and 2.90 Å respectively are

close to the bond lengths: 2.91 Å in $Ba_2Nb_5O_9$ [15], 2.91 Å in $Ba_4Nb_{14}O_{23}$ [11] and 2.89 Å in $Ba_{0.95}NbO_3$ [3, 4].

In all the compounds exhibiting one-dimensionally condensed Nb_6O_{12} clusters, rather short Nb–Nb inter-NbO-block distances are found. The Nb(5)–Nb(5) distance of 3.07 Å in $Ba_3Nb_{16}O_{23}$ is longer than those in $Ba_4Nb_{17}O_{26}$ (3.02 Å), $Ba_4Nb_{14}O_{23}$ (3.02 Å) and $BaNb_5O_8$ (3.04 Å). In the two latter structures extended Hückel calculations have indicated no or very weak Nb–Nb bonding.

The number of valence electrons involved in Nb–Nb bonding in $Ba_3Nb_{16}O_{23}$ is 40 at the ionic limit (Ba^{2+}, Nb^{5+} and O^{2-}). This value is the predicted optimum number obtained via a counting scheme where 3 electrons are assigned to the 8 Nb atoms in the NbO block connecting the Nb_6 octahedra and 2 electrons to the remaining 8 Nb atoms. The model thus assumes 8 Nb^{3+} and 8 Nb^{2+}. A simple but often practical way to determine valences is to calculate Pauling bond order sums according to Brown and Altermatt [23]. The bond order sums for the Nb atoms, coordinated by four O atoms, linking the Nb_6 octahedra are Nb(1) = 2.4, Nb(2) = 2.5 and Nb(3) = 2.2. For the remaining Nb atoms (5-coordination of O atoms) they are Nb(4) = 3.2 and Nb(5) = 2.7. These values fit well with the idea of having Nb^{3+} and Nb^{2+}, keeping in mind that the bond order sum for Nb in NbO is 2.4. The increase in the coordination number of the niobium atoms from 4 to 5 results in additional niobium–oxygen bonding. This gives a reduction in the number of electrons participating in niobium–niobium bonding, *i.e.* those that take part in the formation of a hybridized metallic band, as shown in ref. 24.

6. Conclusions

A new compound $Ba_3Nb_{16}O_{23}$ with an intergrowth structure consisting of quadruple NbO [2∗2∗∞] and triple $BaNbO_3$ {1∗3∗∞} blocks has been synthesized. Its structure and atomic valences conform well with expectations for intergrowth compounds between $BaNbO_3$ and NbO. The formation of $Ba_3Nb_{16}O_{23}$ goes via a disordered intergrowth of $BaNbO_3$ and NbO blocks called the α phasoid. During the synthesis the α phasoid is formed together with NbO at 1350–1450 °C. The amount of NbO decreases at higher synthesis temperatures. High resolution electron microscopy studies show that $Ba_3Nb_{16}O_{23}$ can be recognized as small domains in the α phasoid crystallites found in samples synthesized at 1200 °C. At higher temperatures almost monophasic (X-ray powder diffraction) $Ba_3Nb_{16}O_{23}$ forms. However, HREM reveals the presence of defects, mainly in the form of block size variations.

Acknowledgment

G. Svensson wishes to thank the Swedish Natural Science Research Council for financial support.

References

1 J. Köhler, G. Svensson and A. Simon, *Angew. Chem., 104* (1992) 1463; *Angew. Chem. Int. Edn. Engl., 31* (1992) 1437.
2 R.R. Kreiser and R. Ward, *J. Solid State Chem., 1* (1970) 368.
3 B. Hessen, S.A. Sunshine, T. Siegrist and R. Jimenez, *Mater. Res. Bull., 26* (1991) 85.
4 G. Svensson and P.-E. Werner, *Mater. Res. Bull., 25* (1990) 9.
5 G. Brauer, *Z. Allg. Anorg. Chem., 248* (1941) 1.
6 H. Schäfer and H.-G. Schnering, *Angew. Chem., 76* (1964) 833.
7 J. Köhler, A. Simon, S.J. Hibble and A.K. Cheetham, *J. Less-Common Met., 142* (1988) 123.
8 B. Hessen, S.A. Sunshine, T. Siegrist, A.T. Fiory and J.V. Waszczak, *Chem. Mater., 3* (1991) 528.
9 V.G. Zubkov, V.A. Perelyaev, I.F. Berger, I.A. Kontsevaya, O.V. Makarova, S.A. Turzhevskii, V.A. Gubanov, A.V. Voronin, V.I. Mirmilstein and A.E. Kar'kin, *Sverkhprovod. Fiz., Khim., Tekh., 3* (1990) 2121.
10 G. Svensson, J. Köhler, M.T. Otten and A. Simon, *Z. Anorg. Allg. Chem., 619* (1993) 133.
11 G. Svensson and J. Grins, *Acta Crystallogr., B49* (1993) 626.
12 V.G. Zubkov, V.A. Perelyaev, A.P. Tyutyunnik, I.A. Kontsevaya, D.V. Makarova and G.P. Shweikin, *Rep. Russ. Acad. Sci., 325* (1992) 740.
13 G. Svensson, *Mater. Res. Bull., 23* (1988) 437.
14 V.G. Zubkov, V.A. Perelyaev, I.F. Berger, V.I. Voronin, I.A. Kontsevaya and G.P. Shveikin, *Dokl. Akad. Nauk SSSR, Kristallogr., 312* (1990) 615.
15 G. Svensson, J. Köhler and A. Simon, *J. Alloys Comp., 176* (1991) 123.
16 G. Svensson, J. Köhler and A. Simon, *Angew. Chem. Int. Edn. Engl., 31* (1992) 212; *Angew. Chem., 104* (1992) 192.
17 A. Magnéli, *Microsc., Microanal., Microstruct., 1* (1990) 1.
18 G. Svensson, *Microsc., Microanal., Microstruct., 1* (1990) 343.
19 M.A. O'Keefe, P.R. Buseck and S. Ijima, *Nature (London), 274* (1978) 322.
20 V.P. Glazkov, A.E. Golovin, V.A. Somenkov, S.Sh. Shilstein and I.R. Entin, *Equip. Techn. Exp. (USSR),* (3) (1974) 47.
21 S.A. Howard, *A Program for the Rietveld Analysis of X-Ray and Neutron Powder Diffraction Patterns:* DBW 4.1, University of Missouri-Rolla, 1989.
22 A.K. Cheetham and A.J. Skarnelius, *Anal. Chem., 53* (1981) 1060.
23 I.D. Brown and D. Altermatt, *Acta Crystallogr. B, 41* (1985) 244.
24 V.G. Zubkov, V.A. Perelyaev, I.F. Berger, I.A. Kontsevaya, O.W. Makarova, S.A. Turzhevskii, V.A. Gubanov, V.I. Voronin, A.B. Mirmilstein and A.E. Kar'kin, *Supercond.: Phys. Chem. Techn., 3* (1990) 1969.